ELSEVIER

Surface Science 464 (2000) 272–282

surface science

www.elsevier.nl/locate/susc

First-principles study of (2×1) and (2×2) phosphorus-rich InP(001) surfaces

Olivia Pulci [a,*], Kathy Lüdge [b], W.G. Schmidt [a], F. Bechstedt [a]

[a] *Institut für Festkörpertheorie und Theoretische Optik, Friedrich-Schiller-Universität, Max-Wien Platz 1, D-07743 Jena, Germany*
[b] *Institut für Festkörperphysik, Technische Universität Berlin, Hardenbergstrasse 36, D-10623 Berlin, Germany*

Received 26 May 2000; accepted for publication 11 July 2000

Abstract

The dependence of the InP(001) surface reconstruction on the chemical potentials of its constituents is explored. Based on *first-principles* pseudopotential plane-wave calculations the surface phase diagram is constructed. 17 structural models are studied for the phosphorus-rich InP(001) surfaces, with (2×1), $p(2\times2)$ and $c(2\times2)$ translational symmetry. P-top dimer reconstructions are favoured. Under less P-rich preparation conditions a tendency for disorder is predicted. STM images are also calculated in order to contribute to a solution of the structural puzzle.

Keywords: Density functional calculations; Indium phosphide; Low index single crystal surfaces; Surface electronic phenomena (work function, surface potential, surface states, etc.)

1. Introduction

The understanding of the structure and composition of semiconductor surfaces during growth is one of the keys to controlling the evolution of epitaxial films on the atomic level, for instance using techniques like molecular beam epitaxy (MBE), chemical beam epitaxy (CBE) or metalorganic vapour-phase epitaxy (MOVPE) [1]. This holds in particular for the polar (001) surfaces of III–V semiconductors crystallizing in the zinc-blende structure. Their phases in dependence on substrate temperature and material fluxes, i.e. stoichiometry, have been studied in detail. It is widely accepted that these surfaces reconstruct in such a way that the dangling bonds on the surface cations (III) are unoccupied and those on the surface anions (V) are doubly occupied. This guiding principle, usually referred to as the electron counting rule [2], explains the relatively large reconstructions built up by dimers or missing dimers. This picture of the III–V(001) surfaces is at least well established for the $(2\times4)/c(2\times8)$ and $c(4\times4)$ surface phases of GaAs [3].

In contrast to those of arsenides, the (001) surfaces of other III–V compounds, however, exhibit several peculiarities, which seem to contradict the basic reconstruction mechanism. Whereas AlSb(001) forms an insulating $c(4\times4)$ reconstruction, GaSb possesses (2×10) surfaces that are weakly metallic and, hence, violate the electron counting model [4]. Also the reconstruction mechanism acting on (001) surfaces of phosphides is under discussion. For the InP(001) surface several translational symmetries have been observed. For

* Corresponding author. Fax: +49-3641-947152.
E-mail address: pulci@ifto.physik.uni-jena.de (O. Pulci)

0039-6028/00/$ - see front matter
PII: S0039-6028(00)00729-9

surfaces prepared under MBE, CBE and MOVPE conditions with varying phosphorus partial pressure, (2×4), (2×1) and (2×2) reflection high energy electron diffraction (RHEED) patterns have been monitored for substrate temperatures in the interval 300 to 590°C [5–7] and varying material fluxes. A weak $c(4\times4)$ reconstruction has also been observed at lower temperatures [7,8]. Since P atoms desorb from the surface with increasing temperature, the surface becomes less P-rich. Consequently, the (2×4) phase is known as 'In-rich', whereas lower temperature phases should be represented by 'P-rich' surfaces.

For the In-rich (2×4) phase, images of scanning tunneling microscopy (STM) [9] and results of time-of-flight scattering and recoiling spectrometry [10] have been interpreted as indications for P trimers or a trimerization of the topmost In atoms. However, also P–In–P bridge bonds have been suggested [11,12]. The experimental observations can, however, be described by conventional P–P dimers or mixed In–P dimers as shown recently [13–15].

For the more P-rich phase, STM observations for MOVPE material show that the nominally (2×1) surface, as indicated by low energy electron diffraction (LEED), seems to consist of zig–zag chains along the [110] direction. The corresponding surface geometry has been interpreted as a mixture of $p(2\times2)$ and $c(4\times2)$ domains [16,17], with P–P dimer buckling in-phase [resulting in $p(2\times2)$] or out-of-phase [resulting in $c(4\times2)$]. One expects, however, that buckling is reduced in the presence of ionic bonds. Buckled dimers of identical atoms have only been observed at (001) surfaces of the covalent materials Si and Ge. As and P dimers exhibit practically no buckling on GaAs and InP surfaces [3,9–12]. The observed P-rich surfaces seem to have an overlayer of about 1 ML of P atoms. We will call surfaces of this type '1 ML phases'. Besides dimer buckling, other reasons for the electronic inequivalence of the two P atoms in a dimer, e.g. electron correlation effects between dangling bonds on neighbouring dimers, have been discussed [16]. Very recently, a stabilization of this surface type by alkyl groups and hydrogen atoms has been considered [18,19].

For even more P-rich conditions one approaches a (2×2) phase, which shows only a diffuse boundary with the (2×1) reconstruction [7]. Recently, several observations of this P-rich phase have been published [17–19]. A $(2\times1/2\times2)$ LEED pattern and STM images of a surface with poor long-range ordering have been reported [17–19]. A high number of defects characterize this more P-rich surface, that can only locally be described in terms of P dimers on top of a complete first P layer, giving rise to local (2×2), $c(2\times2)$ and $c(4\times2)$ structures. Observations suggest that this surface contains more than 1 ML of P atoms, possibly up to 2 ML. We call the occurring phases '2 ML phases'.

The present study aims to elucidate the atomic structure of the nominal $(2\times2)/(2\times1)$ InP surfaces in dependence on their preparation. A large variety of models representing (2×1) and (2×2) translational symmetries are analysed. To connect our data energetically with previous theoretical and experimental work, we also include the meanwhile well established mixed-dimer model [13–15,20]. In the extreme P-rich limit we focus our attention on some of the reconstructions that have been proposed [17–19] in order to discuss the experimental findings. We address the question of whether the dimer formation is still appropriate for InP(001) surfaces, where atoms with a remarkable size difference are involved and the bonds are more ionic than in the GaAs case. The validity of the electron counting rule and the dimer buckling are discussed. To that end we perform *first-principles* total-energy (TE) calculations and construct the surface phase diagram. Furthermore, the atomic geometries, surface electronic structures and calculated STM images of the energetically favoured structures are presented.

2. Computational methods

The calculations are based on the density functional theory in the local density approximation (DFT-LDA) [21,22]. A pseudopotential plane-wave code [23,24] is used. The electron–ion interaction is treated by using fully separable, norm-conserving pseudopotentials [25]. The single-particle orbitals are expanded into plane waves up to

an energy cut-off of 15 Ry. The $\boldsymbol{k}$-space integrations are replaced by a sum over eight special points in the irreducible part of the two-dimensional Brillouin zone (BZ) of the (2×2) phases and equivalent sets of points for the larger surface unit cells. The surfaces are modelled using periodic slab geometries along the (001) surface normal. Each unit cell includes an atomic slab with six to seven atomic layers and a vacuum region corresponding to five layers. The cation-terminated bottom layer of the slab is saturated with fractionally charged H atoms [26]. Two layers on this side of the slab are kept frozen, whereas all other atoms are allowed to relax. The minima of the TE functional with respect to both the atomic and electronic degrees of freedom are found by means of a Car–Parrinello molecular dynamical approach [27]. The atoms are assumed to be in their fully relaxed positions when forces acting on the ions are smaller than 0.025 eV/Å. The calculations are performed with the theoretical equilibrium lattice constant of 5.87 Å.

The TE calculations are performed for a variety of structural models, shown in Figs. 1 and 2. In addition to the already known In-rich (2×4) mixed-dimer reconstruction, test structures for the (2×1) and (2×2) reconstructed P-rich InP(001) surfaces with different phosphorus overlayers are considered. The coverages Θ refer to an ideal In-terminated slab. The considered structures realize different P coverages, ranging from $\Theta=0$ for the In-rich (2×4) mixed dimer (Fig. 1) up to $\Theta=2$ in the case of adsorption of eight P atoms on a (2×2) cell (Fig. 2). We consider adsorption on the In-terminated InP(001) surface with P coverage $\Theta\leq1$ as shown in Fig. 1, and with $1<\Theta\leq2$ as shown in Fig. 2. As reconstruction elements in the adlayer we consider mixed dimers (md) in parallel (p) or antiparallel (a) configurations, buckled and unbuckled top-P dimers (td), possibly in a staggered arrangement (s), and phosphorus adatoms (aa). The mixed dimer structures md$i$ represent either an In–P dimer on the indium-terminated surface ($i=1$) or an In–P dimer on top of a complete P adsorbate layer ($i=2$). The (2×2) top-P dimer and adatom structures, td$i$ and aa$i$, correspond to a coverage of half a P monolayer ($\Theta=0.5$) for $i=1$ (Fig. 1), and of one and a half

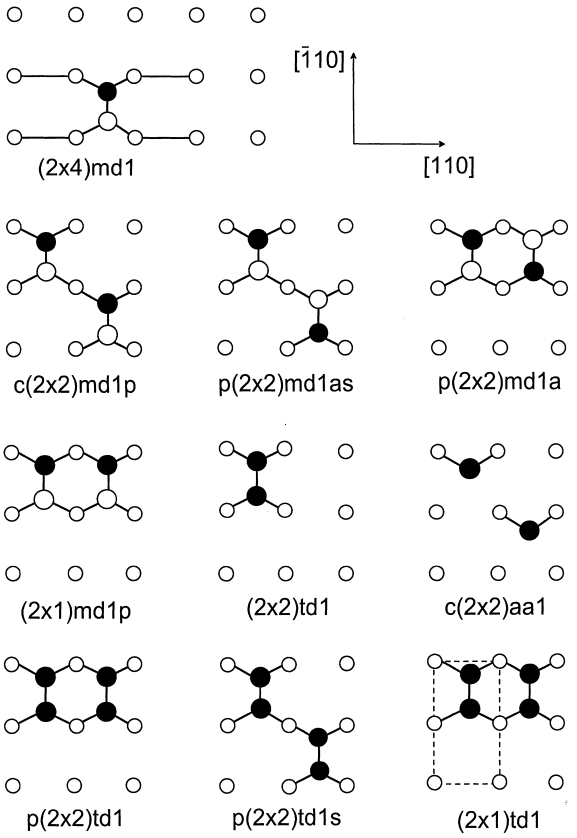

Fig. 1. Top view of surface structures with P coverages Θ less than 1 ML. Different arrangements of mixed dimers (md) and top-P dimers (td) as well as single P adatoms (aa) are considered. In the case of two md dimers per (2×2) surface unit cell parallel (p) or antiparallel (a) arrangements are distinguished. Two dimers can form a staggered (s) arrangement. Filled circles: P atoms; open circles: In atoms.

monolayers ($\Theta=1.5$) for $i=2$ (Fig. 2). The $p(2\times2)$ top-dimer adsorbates td1 and td1s (Fig. 1) stand for complete P monolayers with $\Theta=1$, where 's' indicates a staggered dimer configuration. The $p(2\times2)$td2 and $p(2\times2)$td2s, shown in Fig. 2, represent two top-dimer adsorbates on a complete P monolayer ($\Theta=2$).

Because of the variation of the number of surface atoms in the unit cell, the energetical comparison of the structures in Figs. 1 and 2 depends on the chemical potentials $\mu(X)$ of the surface constituents X= P, In [28]. In the zero-temperature limit this corresponds to the study of the surface energy Ω versus the chemical potential

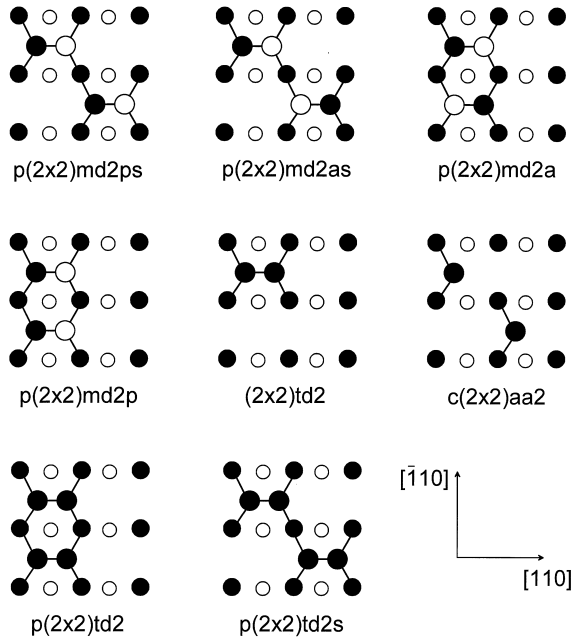

Fig. 2. As Fig. 1 but for P coverages Θ between 1 and 2 ML ($1<\Theta\leq 2$).

of one constituent. Since bulk solid InP with the chemical potential $\mu^{\text{bulk}}(\text{InP})$ is a reservoir which can exchange atoms with the surface, the mass action law, $\mu(\text{In})+\mu(\text{P})=\mu^{\text{bulk}}(\text{InP})$, holds. It allows the representation of the surface energy Ω as a function of $\mu(\text{In})$ or $\mu(\text{P})$. The bulk energy per pair, $\mu^{\text{bulk}}(\text{InP})=\mu^{\text{bulk}}(\text{In})+\mu^{\text{bulk}}(\text{P})-\Delta H_{\text{f}}(\text{InP})$, is equal to the sum of the energies of the bulk elemental In and P minus the heat of formation $\Delta H_{\text{f}}(\text{InP})$. Elemental In occurs in the form of a bulk tetragonal metal with $\mu^{\text{bulk}}(\text{In})$. Elemental phosphorus shows a wide structural variety, the most common allotropes being the white, black, violet and red phosphorus and some amorphous forms. For the formation of InP from white phosphorus, the solid high-temperature phase, the experimental value amounts to $\Delta H_{\text{f}}(\text{InP})=0.92$ eV for the heat of formation [29].

The chemical potential of each element cannot be above that of the bulk elemental phase being stable at the substrate temperature. It approaches the elemental bulk chemical potential in the case that bulk material is present and the surface is in equilibrium with the elemental condensed bulk phase. It is below the bulk chemical potential in the cases where the elemental bulk is not stable and the surface is in equilibrium with a gaseous phase, e.g. the gas of two atomic molecules P_2. According to the mass action law and the definition of the heat of formation, the chemical potential $\mu(\text{In})$ varies between the value for the corresponding metal $\mu^{\text{bulk}}(\text{In})$ and a value $\mu^{\text{bulk}}(\text{In})-\Delta H_{\text{f}}(\text{InP})$ reduced by the heat of formation of the compound InP. With $\Delta\mu(\text{In})=\mu(\text{In})-\mu^{\text{bulk}}(\text{In})$, it holds that $-1\leq\Delta\mu(\text{In})/\Delta H_{\text{f}}(\text{InP})\leq 0$. Extreme In-rich (P-poor) preparation conditions are described by $\Delta\mu(\text{In})=0$, whereas $\Delta\mu(\text{In})=-\Delta H_{\text{f}}(\text{InP})$ characterizes more P-rich (In-poor) conditions.

The surface energy Ω is represented in Fig. 3 versus the variation $\Delta\mu(\text{In})$ of the In chemical potential with respect to its bulk value. Since, due to the various possible modifications, the white phosphorus does not unambiguously define the elemental condensed bulk phase in equilibrium with the surface and, moreover, the heat of forma-

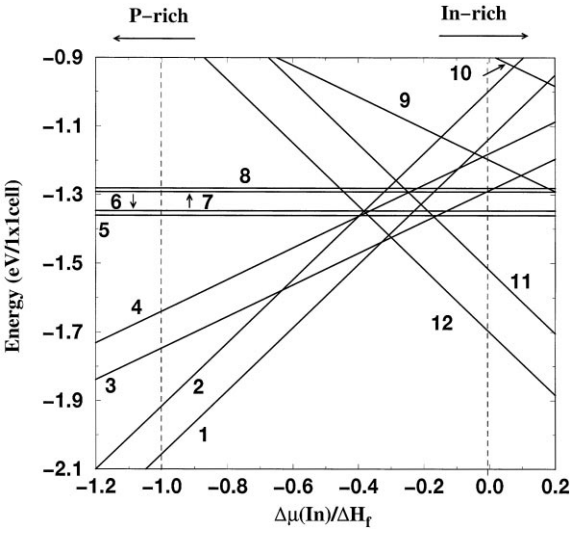

Fig. 3. Surface energy (with respect to the ideal unrelaxed P-terminated surface) per (1×1) unit cell versus the variation of the In chemical potential. The thermodynamically allowed range is given by $-1\leq\Delta\mu(\text{In})/\Delta H_{\text{f}}\leq 0.0$. The energetically most favourable surface reconstruction models are shown. 1: $p(2\times 2)$td2; 2: $p(2\times 2)$td2s; 3: (2×2)td2; 4: $c(2\times 2)$aa2; 5: $p(2\times 2)$td1; 6: $p(2\times 2)$md2ps; 7: $p(2\times 2)$td1s; 8: (2×1)td1; 9: (2×2)td1; 10: $c(2\times 2)$aa1; 11: (2×1)md1p; 12: (2×4)md1.

tion ΔH_f(InP) varies with temperature [30], we have also checked the influence of different values of ΔH_f(InP) on the phase diagram in Fig. 3. There is, however, only an influence on the thermodynamically allowed range without major consequences on the stability of the different surface phases.

3. Results

3.1. Geometry and bonding

3.1.1. Geometries with ≤ 1 ML phosphorus

The surfaces with P coverage $\Theta \leq 1$ and four or less adatoms per (2×2) unit cell are shown in Fig. 1. They may represent reconstruction elements occurring in the surface phases experimentally prepared under intermediate P-rich conditions [16,17]. This holds in particular for the pure P adlayers.

However, any attempt to buckle the top-P dimer (td1) structures failed within the (2×1), (2×2) and $p(2\times2)$ translational symmetries. We found local minima on the Born–Oppenheimer TE face only for unbuckled top dimers. This is in agreement with findings for dimers of equal atoms at other (001) surfaces of III–V compounds [3,13–15]. Dimer buckling increases the electrostatic energy of the system and, hence, is unlikely in the presence of partially ionic bonds. Our TE calculations thus do not confirm the existence of buckled dimers used to explain the zig–zag chains observed by STM for intermediate P coverages [16,17]. Another possibility for the formation of zig–zag chains along the [110] direction could be a corresponding arrangement of phosphorus atoms in the adlayer structure aa1 in Fig. 1. This $c(2\times2)$ overlayer is characterized by a zig–zag arrangement of two P atoms on top of a complete In layer. However, this adatom structure is unstable. If we instead allow the formation of a dimer, i.e. the (2×2)td1 structure in Fig. 1, the energy decreases by about 0.3 eV per atom. The complete coverage of the In-terminated (001) surface by top-P dimer td1 with $p(2\times2)$td1 or $p(2\times2)$td1s translational symmetries offers further possibilities for the formation of chain structures. The two dimers per unit cell become inequivalent; for that reason no $c(2\times2)$ symmetry occurs in the staggered case. The two P dimers occur at different distances of about 2.2 Å on average from the underlying In atomic layer. As a consequence, the surface becomes semiconducting. The hybridization of the dangling bonds tends towards s and p (p_z and sp^2_{xy}) for upper (lower) dimers. Four and six electrons are accommodated on the σ- and π-states of the corresponding dimer. Another possibility to explain zig–zag chains along [110] are mixed dimers of P and In atoms which are automatically buckled [13–15]. In the '1 ML' framework we consider four mixed-dimer (md) overlayers with $c(2\times2)$ and $p(2\times2)$ reconstructions [which correspond to (2×1) in the case of a parallel arrangement of the two dimers] (cf. Fig. 1). Among these mixed-dimer geometries, the energetically most favourable one is the md1p structure, consisting of two identical parallel In–P dimers per $p(2\times2)$ cell on an In layer and, hence, describing in reality a 2×1 reconstruction. The dimer buckling amounts to 0.48 Å, with the P atoms moving out of the surface and the In ones down towards the bulk. However, the resulting equal arrangement of P and In adatoms can only explain linear chains. Moreover, experimental findings from infrared spectroscopy rule out the possibility of In atoms on the top of the surface [16]. Also, the observation of the dimer flipping seems to conclusively rule out mixed dimers [17]. In order to explain the obvious discrepancies between theory and experiment, at least for the $p(2\times2)$ translational symmetry observed in STM and assumed in the TE calculations, other reasons have to be considered, for instance a defect stabilization of local structures at real surfaces, adsorption of further species, such as hydrogen, or electron correlation effects.

3.1.2. Structures with >1 ML phosphorus

The surfaces with more than one monolayer of P are shown in Fig. 2. We have considered several possible dimer reconstructions and adatom arrangements, ranging from 1.5 to 2 ML of P and exhibiting a $p(2\times2)$ or $c(2\times2)$ translational symmetry. The (2×2)td2 structure (Fig. 2) has just one P dimer per (2×2) cell, on top of a complete P monolayer ($\Theta=1.5$). It is buckled with a buck-

ling amplitude of 0.69 Å. The driving forces for this reconstruction seem to be the same as in the case of Si and Ge(001) surfaces of bulk systems with a small energy gap [31]. A charge transfer from the lower to the upper P atom of the dimer occurs. Nevertheless, the buckled dimers cannot explain the observed zig–zag rows since each second dimer is missing. The c(2×2)aa2 structure (Fig. 2), with the same surface stoichiometry but without dimer bonds between the two extra P adatoms on top of the complete P monolayer, is also unstable. This structure is about 0.1 eV/atom higher in energy than the (2×2)td2 one, thus showing that the dimer formation is always energetically more favourable. The two top-P dimer structures p(2×2)td2 and p(2×2)td2s with $\Theta=2$ (Fig. 2) show again no buckling. In contrast to the case of smaller coverage, e.g. $\Theta=1.5$ represented by (2×2)td2, the dimer–dimer interaction makes buckling unfavourable. The insulating character of the surface is again a consequence of the geometrical and electronic inequivalence of the two dimers. As in the monolayer case, they differ with respect to the distance from the underlying complete P layer and with respect to their dimer lengths. These vertical and horizontal differences are 0.30 Å and 0.57 Å for the p(2×2)td2 structure, and 0.64 Å and 1.00 Å for the p(2×2)td2s one. The two dimers can accommodate eight and six electrons, hence the surface can be semiconducting. On the other hand, the mixed-dimer structures md2, with parallel and antiparallel arrangement of the dimers and p(2×2) translational symmetry (Fig. 2), show a significant buckling. Among them, the energetically most favourable one is the p(2×2)md2as structure with In–P buckling of about 0.6 Å.

As an example for the characteristic arrangement of the phosphorus atoms in the two atomic layers of the P adsorbate, we discuss the two reconstructions p(2×2)td2 and p(2×2)td2s with a P coverage of $\Theta=2$ in more detail. The most important geometry parameters are listed in Table 1 and defined in Fig. 4. The interesting point is that the reconstruction is not only characterized by the formation of two P dimers in the uppermost P layer with different distances to the In termination of the bulk. Rather, there is also a remarkable displacement of the dimers parallel to the $[\bar{1}10]$ direction. Consequently, bonds between the dimer displaced outward and the second atomic layer are stretched considerably. Actually, the distances $L=$ 3.3 and 3.6 Å are too long for covalent bonds. A typical measure of a bond is the sum of the covalent radii, about 2.12 Å. On the other hand, the bonds of the dimers displaced towards the bulk and the second atomic layer are shortened to $l=2.0$ or 2.30 Å. A similar trend is observed for the dimer bond lengths of $d_1=2.4/2.61$ Å in the lower dimers and $d_2=2.1$ Å in the upper dimers. There seems to be a tendency for a two-fold coordination of the atoms in the uppermost P layer. Each P atom possesses two strong bonds and a weak bond. In the second atomic layer this tendency is accompanied by the trend of a three-fold coordination of half of the atoms. Altogether, the adlayer shows features known from solid black phosphorus consisting of bilayers, where a P atom has three nearest neighbours at about 2.2 Å and the minimum P–P distance in adjacent layers amounts to 3.8 Å.

3.2. Phase diagram

In Fig. 3 we plot the surface energies Ω of the energetically most favourable structures versus the In chemical potential in an interval slightly larger than the allowed range. The ideal unrelaxed surface

Table 1
Structural parameters (Å) for P-rich InP(001) surfaces with p(2×2)td2 and p(2×2)td2s geometry. The parameters are explained in Fig. 4

	Δ_{1z}	Δ^{*}_{1z}	Δ_{2z}	Δ_{3z}	δ	d_{12}	L	l	d_1	d_2
p(2×2)td2	1.32	1.15	1.29	1.56	0.16	4.82	3.25	2.02	2.40	2.08
p(2×2)td2s	1.13	1.47	1.67	1.17	0.34	5.13	3.64	2.27	2.61	2.08

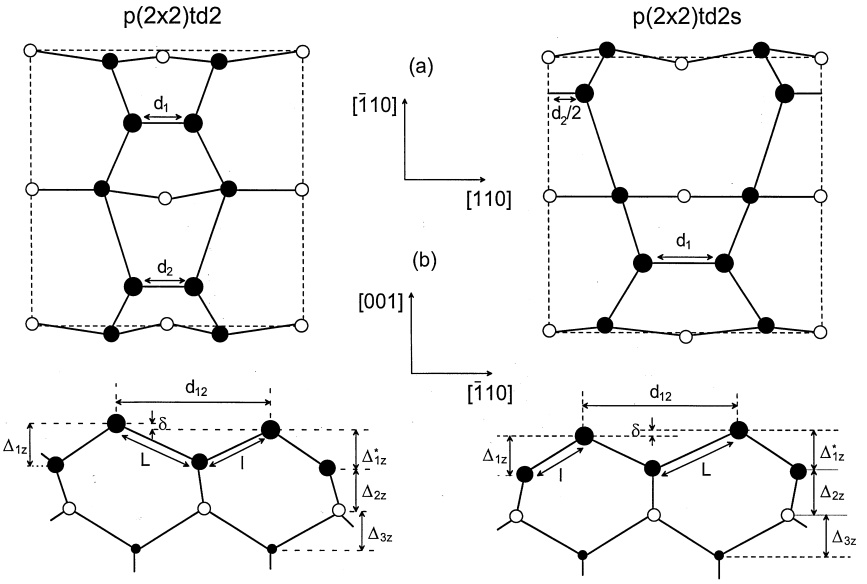

Fig. 4. Top (a) and side (b) view of the P-rich ($\Theta=2$) InP(001) surfaces with p(2×2)td2 and p(2×2)td2s geometries. Open (filled) circles are In (P) atoms. The largest size of circles indicates the topmost layer.

with one complete P layer is used as energy zero. The surface phase diagram of InP(001) also includes the (2×4) boundary of the In-rich phase. It is known [13–15] that under In-rich preparation conditions the (2×4) reconstruction is represented by a single mixed dimer on top of the In-terminated surface (cf. Fig. 1). The phase diagram shows that under more P-rich conditions, (2×2) overlayer structures with 2 or 1.5 ML P become more favourable. In the framework of the restriction to (2×2) translational symmetries, several different surface geometries can be distinguished in dependence on the chemical potential of In. Under the most P-rich conditions the p(2×2)td2 reconstruction is the most energetically favourable one. The staggered arrangement of the two P dimers, the p(2×2)td2s structure, is close in energy. Therefore its existence cannot be excluded. Defect-induced strain fields may stabilize other arrangements of the surface dimers. However, all favourable structures under P-rich conditions should contain two P monolayers with different P–P dimers in the uppermost atomic layer.

Vogt et al. [17] and Hicks and coworkers [18,19] observed for very P-rich growth conditions a mixture of domains of c(4×2), (2×2) and c(2×2) translational symmetry. However, a complete comparison of experimental and theoretical results is hardly possible. On the one hand, disorder effects play an essential role. STM images indicate a random distribution of the local structures and many defects [17]. Hence, long-range order is absent, in contrast to the assumption in the TE calculations. Furthermore, in particular during the MOVPE growth of the P-rich InP(001) surfaces, alkyl groups and H atoms adsorb onto the P overlayer [18,19]. The adsorption onto half of the exposed phosphorus atoms in the uppermost layer may completely change the reconstruction behaviour.

The situation becomes even more complicated in an intermediate range of P-rich surface preparation conditions with $\Delta\mu(\mathrm{In})/\Delta H_f(\mathrm{InP})$ between -0.3 and -0.5 (cf. Fig. 3). The TE calculations indicate a tendency for coexistence of several surface phases of different structure and stoichiometry, at least the two top-P dimer structure p(2×2)td2 with $\Theta=2$, the one top-P dimer structure (2×2)td2 with $\Theta=1.5$, and the one mixed-dimer structure (2×4)md1 with $\Theta=0$. However, also a variety of other structures are close in energy. They involve the mixed-dimer structures

on top of a P layer [e.g. p(2×2)md2ps in Fig. 2], as well as the P monolayer structures td1 with p(2×2) or (2×1) translational symmetry (Fig. 1). All these structures represent a $\Theta = 1$ surface stoichiometry. The similarity of their surface energies indicates that randomness may reduce the free energy of the surface system for a given substrate temperature T. A configurational entropy of about $2k_B$ may already give a lowering of the free energy by about 0.1 eV per (1×1) unit cell at a temperature of about 600 K. Consequently, taking into consideration the error bars of the calculations, we cannot exclude the coexistence of several structural elements on one and the same surface: unbuckled P dimers on a P monolayer, buckled dimers on a P monolayer, mixed dimers on a P monolayer, unbuckled P dimers on the In termination, and mixed dimers on the In termination. These structural elements can be combined to form local arrangements, which may then give p(2×2), c(2×2) and (2×1) translational symmetries.

Our calculations do not confirm the STM interpretation of the intermediate phase in terms of one monolayer of buckled P–P dimers [16,17]. The TE optimizations of the ideal surfaces show that dimer buckling is energetically unfavourable, as for other surfaces of polar semiconductors. According to our calculations, buckled dimers only occur for the missing-dimer (2×2)td2 and for mixed-dimer structures. This indicates a discrepancy between theoretical results and STM findings for intermediate variations of the In chemical potentials [16]. The P zig–zag chains being in-phase [generating p(2×2)] or out-of-phase [generating c(4×2)] on an In atomic layer cannot be realized since the buckling of these dimer-related structures is unstable. However, there is an additional problem. The semiconducting character of such a surface [16] needs further consideration. With two exceptions [(2×1)td1 and (2×2)td1 in Fig. 1], all overlayer structures studied theoretically fulfil the electron counting rule and, hence, give rise to an insulating behaviour of the surface. However, this is not automatically the case for zig–zag chain arrangements of, apart from the orientation, equally buckled P dimers derived from the STM studies [16,17]. Additional effects may be involved, for instance effects of strong electron correlation. Since the dimer interaction is weak, the dispersion of the electronic surface-state bands related to the π- and π*-dimer states is nearly vanishing. Consequently, a Mott–Hubbard mechanism may correlate the electrons as recently observed for Si-rich SiC(0001) surfaces [32]. Other effects are also possible. The obviously different electron occupation of the two dimer atoms may also be related to a negative-U behaviour as predicted for alkali-covered GaAs(110) surfaces [33]. In order to check this idea, spin-polarized calculations need to be performed.

3.3. Band structures

In Fig. 5 the surface-state energy bands of the energetically most favourable P-rich structures, the p(2×2)td2 (Fig. 5a) and the p(2×2)td2s (Fig. 5b), are shown together with the projected InP bulk band structure. Both surfaces are semiconducting. In both cases, V_1, the highest occupied surface band, lies slightly above the bulk valence band maximum (VBM). The maximum occurs at the J–K line (closer to J) of the surface BZ. Empty surface-related bands also appear in the fundamental gap. The lowest band, C_1, exhibits one pronounced minimum on the Γ–J′ line near J′. The other extremum at Γ corresponds more to a saddle point in the p(2×2)td2 case, whereas it is a minimum in the p(2×2)td2s case. Consequently, both surfaces possess an indirect gap J→J′ [p(2×2)td2] or J→Γ [p(2×2)td2s]. The gap energies are 0.60 and 0.45 eV. In Fig. 6 we discuss the orbital character of the two lowest empty (C_1, C_2) and the two highest occupied surface bands (V_1, V_2) at the K point. As a consequence of the stretching of the back bonds, practically dangling bond-like surface states occur at the second layer P atoms. In the p(2×2)td2 case, the maximum of V_1 occurs between J and K about 0.3 eV above the VBM. This band is related to the occupied dangling bonds (p_z-like) of the P atoms in the second layer, since the bond to the uppermost dimer is extremely weak. Also V_2 is related to these dangling bonds. Additionally, antibonding π* orbitals at the lower dimer and backbonds contribute strongly. The lowest empty surface band, C_1, is related to antibonding σ*-like orbitals located

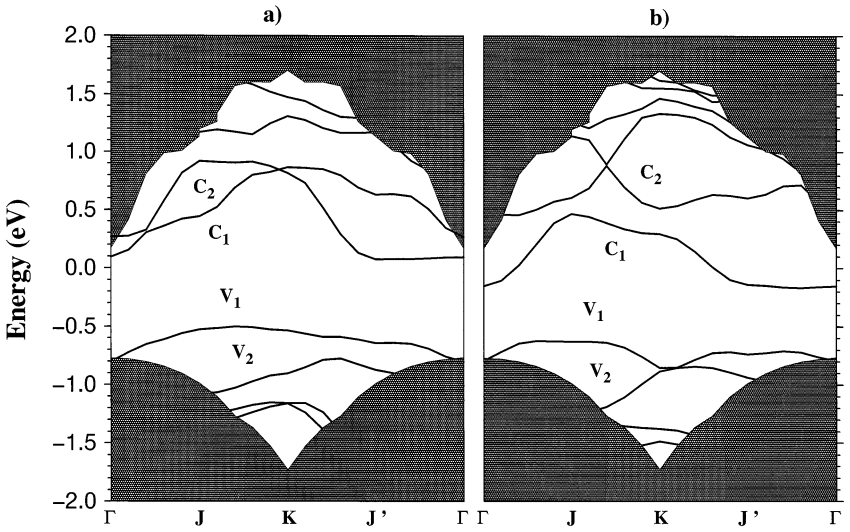

Fig. 5. Surface band structure for the p(2×2)td2 (a) and p(2×2)td2s (b) surfaces. Grey regions indicate the projected bulk band structure.

at the lower dimer. The state belonging to the higher band, C_2, at K is an antibonding state localized at the uppermost dimer (see Fig. 6a).

In the p(2×2)td2s case, V_1 is, around J, about 0.5 eV above the VBM. Also for this structure V_1 is a dangling bond state of the P atoms at the second layer, but also an antibonding orbital π^*-like of the lower dimer does contribute. The orbital corresponding to V_2 has mainly a mixed $\sigma+\pi^*$ character, located at the lower dimer (see Fig. 6b), but also the dangling bonds of the second P layer do contribute (not shown in the figure). The empty surface states C_1 and C_2 are antibonding combinations of orbitals of the upper and lower dimer, respectively.

From the analysis of these states, it is clear that a picture of the dimer states as purely σ, π, σ^* and π^* orbitals is oversimplified. Moreover, the uppermost dimer has two rather weak bonds with the P atoms at the second layer, as shown by the dangling bond character of V_1 and V_2. Also the interpretation of the other surface states lying in the gap is quite difficult, since many contributions from dimer and backbond states appear.

3.4. STM images

The fact that in several STM images of the most P-rich phase local (2×2), c(2×2) and c(4×2) [16–19] domains are observed may be traced back to the different geometry and electronic structure of the two top dimers in a (2×2) cell. In order to investigate this idea, we have performed calculations of STM images for the most phosphorus-rich dimerized overlayer structures (2×2)td2, p(2×2)td2 and p(2×2)td2s (cf. Fig. 2). Calculating the STM images we use the same approach as in Ref. [34]. In this approach the tunneling current is proportional to the spatially resolved density of states integrated over a certain energy interval. Depending on the number of either empty or occupied energy bands one can simulate STM images corresponding to different voltages applied to the sample with respect to the tip.

Results for images of the occupied states are plotted in Fig. 7. We have integrated states over an energy interval of 1.5 eV below the VBM in order to simulate a negative bias of about 2.5 V. The simulated STM images mainly show the occupied dimer states. The buckling of the top dimer in the missing-dimer structure (2×2)td2 in Fig. 7a gives rise to a square lattice of the STM spots. In the case of the p(2×2)td2 structure rows of dimers with different intensity can be seen along the $[\bar{1}10]$ direction. Indications for these reconstructions are not seen experimentally [16–19]. Interestingly,

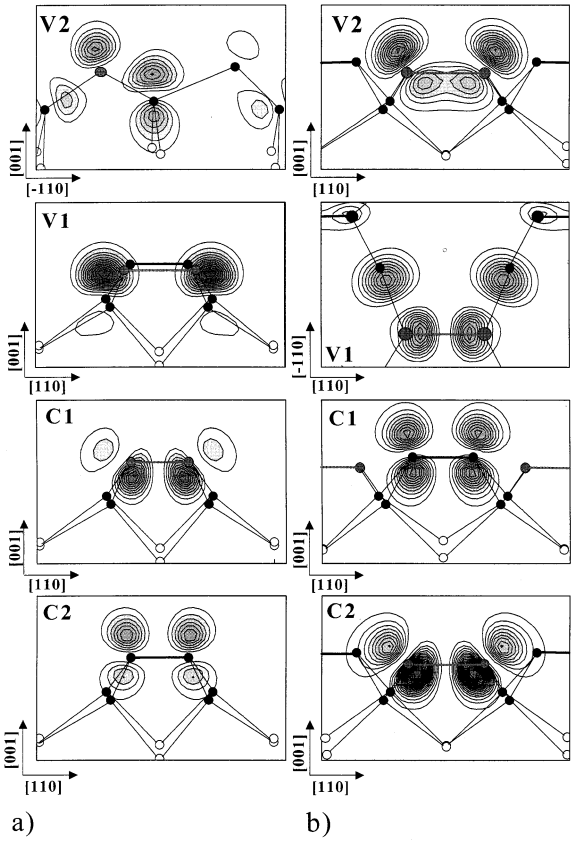

Fig. 6. Contour plots of the squared wave functions at K for highest occupied (V_1, V_2) and lowest unoccupied (C_1, C_2) surface states. (a) p(2×2)td2; (b) p(2×2)td2s. The states are plotted in a ($\bar{1}$10) plane (side view), with the exception of V_2 (a), plotted in the (110) plane, and V_1(b), plotted in the (001) plane (top view). Grey circles indicates P atoms in the lower dimer.

in-phase zig–zag chains along [110] occur in the p(2×2)td2s case. This allows an interpretation of the experimental findings, provided that each dimer gives only one oval spot due to the limited experimental resolution. Then, at least the in-phase zig–zag chain structures observed by Vogt et al. [17] and Hicks and coworkers [18,19] for extremely P-rich preparation conditions could be explained.

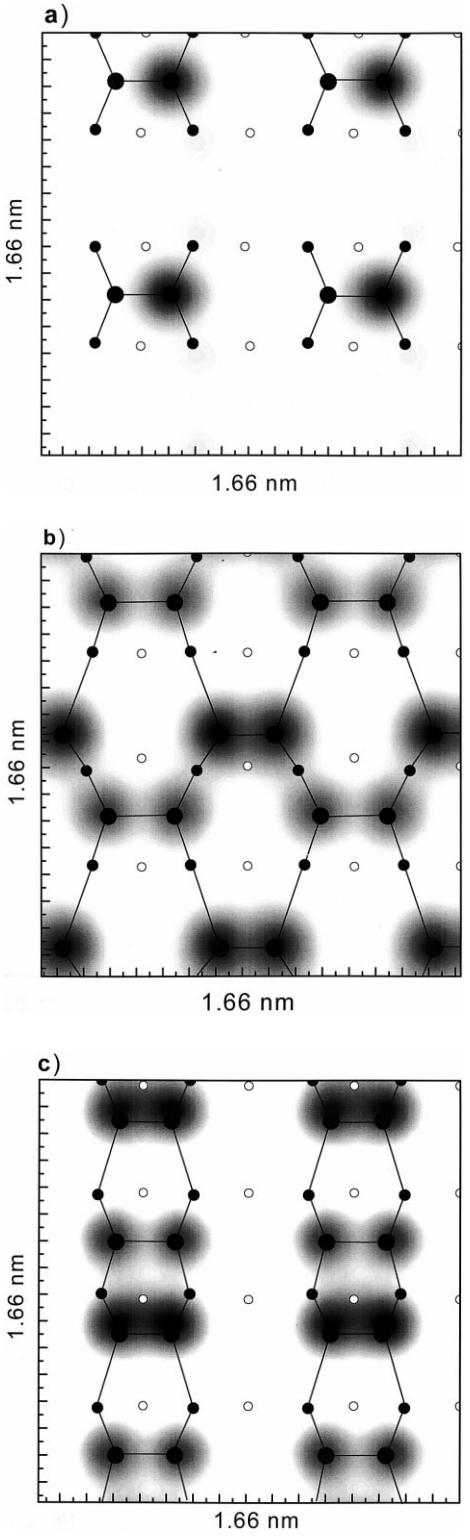

Fig. 7. Filled state STM images calculated for the (2×2)td2 (a), p(2×2)td2 (b) and p(2×2)td2s (c) top-P dimer geometries, shown in Figs. 2 and 4. The dimer bonds are along the [110] direction.

4. Conclusions

We have presented a comprehensive study of the structure as well as energetics and the accompanying ab initio thermodynamics of the reconstructed polar (001) surfaces of the InP for different phosphorus-rich conditions, focusing on the small reconstructions in (2×2) cells. The surface preparation conditions are taken into account by the variation of the P coverage of the surface, ranging from 0 to 2 ML. Under P-rich conditions the surface reconstructions are governed by P–P dimers. No clear evidence for mixed dimers appears. Only under In-rich conditions [(2×4) reconstruction] is a mixed dimer on top of a complete In layer favourable. Under P-rich conditions the $p(2\times2)$ and (2×2) reconstructions, all containing P–P dimers, dominate. The staggered $p(2\times2)$td2s structure can explain the STM images published recently, whereas the (2×2) surface, being buckled, gives the right symmetry, but cannot explain the STM spots observed experimentally. No experimental observation of the $p(2\times2)$td2 has been reported until now. The electronic structure of the P–P dimers occurring under P-rich conditions needs further study, including strong electron correlation effects. Moreover, the inclusion of disorder by means of larger supercells seems to be essential.

Acknowledgements

Helpful discussions with P. Vogt and N. Esser are gratefully acknowledged. This work was financially supported by the Deutsche Forschungsgemeinschaft (Contract No. Be 1346/10-1). Part of the calculations were done using the computer facilities of the J. v. Neumann Institut Jülich.

References

[1] Z. Zhang, M.G. Lagally, Science 276 (1997) 377.
[2] M.D. Pashley, Phys. Rev. B 40 (1989) 10 481.
[3] Q.-K. Xue, T. Hashizume, T. Sakurai, Progr. Surf. Sci. 56 (1997) 1 and references cited therein.
[4] L.J. Whitman, P.M. Thibado, S.C. Erwin, B.R. Bennett, B.V. Shanabrook, Phys. Rev. Lett. 79 (1997) 693.
[5] B.X. Yang, H. Hasegawa, Jpn. J. Appl. Phys. 33 (1994) 742.
[6] B. Junno, S. Jeppesen, M.S. Miller, L. Samuelson, J. Cryst. Growth 164 (1996) 66.
[7] K.B. Ozanyan, P.J. Parbrook, M. Hopkinson, C.R. Whitchouse, Z. Sobiesierski, D.I. Westwood, J. Appl. Phys. 82 (1997) 474.
[8] M. Zorn, T. Trepk, J.-T. Zettler, B. Junno, C. Meyne, K. Knorr, T. Wethkamp, M. Klein, M. Miller, W. Richter, L. Samuelson, Appl. Phys. A: Mater. Sci. Process. 65 (1997) 333.
[9] C.D. MacPherson, R.A. Wolkow, C.E.J. Mitchel, A.B. McLean, Phys. Rev. Lett. 77 (1996) 691.
[10] M.M. Sung, C. Kim, H. Bu, D.S. Karpuzov, J.W. Rabelais, Surf. Sci. 322 (1996) 116.
[11] J.-M. Lin, L.J. Lewis, Surf. Sci. 325 (1995) 251.
[12] H. Seong, L.J. Lewis, Surf. Sci. 337 (1995) 166.
[13] W.G. Schmidt, F. Bechstedt, N. Esser, M. Pristovsek, Ch. Schultz, W. Richter, Phys. Rev. B 57 (1998) 14 596.
[14] W.G. Schmidt, F. Bechstedt, Surf. Sci. 409 (1998) 474.
[15] W.G. Schmidt, E.L. Briggs, J. Bernholc, F. Bechstedt, Phys. Rev. B 59 (1999) 2234.
[16] L. Li, B.-K. Han, Q. Fu, R.F. Hicks, Phys. Rev. Lett. 82 (1999) 1879.
[17] P. Vogt, Th. Hannappel, S. Visbeck, K. Knorr, N. Esser, W. Richter, Phys. Rev. B 60 (1999) R5117.
[18] L. Li, B.-K. Han, C.H. Li, Q. Fu, R.F. Hicks, Appl. Phys. Lett. 75 (1999) 683.
[19] L. Li, Q. Fu, C.H. Li, B.-K. Han, R.F. Hicks, Phys. Rev. B 61 (2000) 10 223.
[20] S. Mirbt, N. Moll, K. Cho, J.D. Joannopoulos, Phys. Rev. B 60 (1999) 13 283.
[21] P. Hohenberg, W. Kohn, Phys. Rev. B 136 (1964) 864.
[22] W. Kohn, L.J. Sham, Phys. Rev. A 140 (1965) 1133.
[23] R. Stumpf, M. Scheffler, Comput. Phys. Commun. 79 (1994) 447.
[24] M. Bockstedte, A. Kley, J. Neugebauer, M. Scheffler, Comput. Phys. Commun. 107 (1997) 187.
[25] D.R. Hamann, Phys. Rev. B 40 (1989) 2980.
[26] K. Shiraishi, J. Phys. Soc. Jpn. 59 (1990) 3455.
[27] R. Car, M. Parrinello, Phys. Rev. Lett. 55 (1985) 2471.
[28] G.-X. Qian, R.M. Martin, D.J. Chadi, Phys. Rev. Lett. 60 (1988) 162, Phys. Rev. B 38 (1988) 7649.
[29] D.R. Lide (Ed.), CRC Handbook of Chemistry and Physics, seventy seventh edn., CRC Press, Boca Raton, FL, 1996.
[30] I. Barin, Thermochemical Data of Pure Substances, VCH, Weinheim, 1995.
[31] H. Krüger, J. Pollmann, Phys. Rev. Lett. 74 (1995) 1155.
[32] J. Furthmüller, F. Bechstedt, H. Hüsken, B. Schröter, W. Richter, Phys. Rev. B 58 (1998) 13 712.
[33] O. Pankratov, M. Scheffler, Phys. Rev. Lett. 70 (1993) 351, Phys. Rev. Lett. 71 (1993) 2797.
[34] K. Lüdge, P. Vogt, O. Pulci, N. Esser, F. Bechstedt, W. Richter, Phys. Rev. B (2000) submitted.